



**HAL**  
open science

## Multiphysics thermal design of a high-speed permanent-magnet machine

Zlatko Kolondzovski, Anouar Belahcen, Antero Arkkio

► **To cite this version:**

Zlatko Kolondzovski, Anouar Belahcen, Antero Arkkio. Multiphysics thermal design of a high-speed permanent-magnet machine. *Applied Thermal Engineering*, 2009, 29 (13), pp.2693. 10.1016/j.applthermaleng.2009.01.001 . hal-00539083

**HAL Id: hal-00539083**

**<https://hal.science/hal-00539083>**

Submitted on 24 Nov 2010

**HAL** is a multi-disciplinary open access archive for the deposit and dissemination of scientific research documents, whether they are published or not. The documents may come from teaching and research institutions in France or abroad, or from public or private research centers.

L'archive ouverte pluridisciplinaire **HAL**, est destinée au dépôt et à la diffusion de documents scientifiques de niveau recherche, publiés ou non, émanant des établissements d'enseignement et de recherche français ou étrangers, des laboratoires publics ou privés.

## Accepted Manuscript

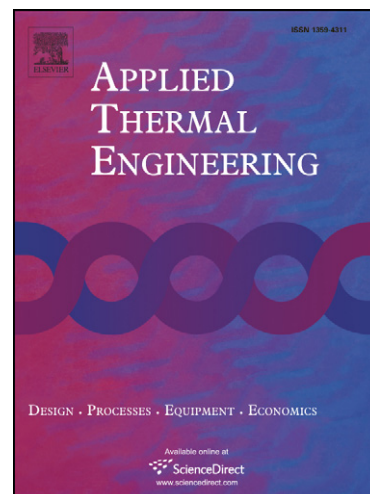
Multiphysics thermal design of a high-speed permanent-magnet machine

Zlatko Kolondzovski, Anouar Belahcen, Antero Arkkio

PII: S1359-4311(09)00003-9  
DOI: [10.1016/j.applthermaleng.2009.01.001](https://doi.org/10.1016/j.applthermaleng.2009.01.001)  
Reference: ATE 2715

To appear in: *Applied Thermal Engineering*

Received Date: 5 January 2008  
Revised Date: 3 July 2008  
Accepted Date: 3 January 2009



Please cite this article as: Z. Kolondzovski, A. Belahcen, A. Arkkio, Multiphysics thermal design of a high-speed permanent-magnet machine, *Applied Thermal Engineering* (2009), doi: [10.1016/j.applthermaleng.2009.01.001](https://doi.org/10.1016/j.applthermaleng.2009.01.001)

This is a PDF file of an unedited manuscript that has been accepted for publication. As a service to our customers we are providing this early version of the manuscript. The manuscript will undergo copyediting, typesetting, and review of the resulting proof before it is published in its final form. Please note that during the production process errors may be discovered which could affect the content, and all legal disclaimers that apply to the journal pertain.

**MULTIPHYSICS THERMAL DESIGN OF A HIGH-SPEED  
PERMANENT-MAGNET MACHINE**

Zlatko Kolondzovski\*, Anouar Belahcen and Antero Arkkio

Helsinki University of Technology, Laboratory of Electromechanics  
P.O. Box 3000, FI-02015 TKK, Finland

**Abstract:** In the paper, different methods for thermal design of a high-speed permanent-magnet machine are presented. The first implemented method is a numerical-multiphysics method which couples computational fluid dynamics and heat-transfer equations. The geometry of the machine in this method is considered to be 2D axi-symmetric. This method gives simultaneous solutions for the turbulent properties of the cooling fluid as well as for the temperature rise in the fluid and solid domains of the machine, but it is primarily intended for solving the fluid domain. The distribution of the temperature rise in the solid domain of the machine is estimated with a 3D numerical heat-transfer method that is the second one implemented in this paper. This method uses the properties of the turbulent flow from the 2D multiphysics method such as the temperature rise of the fluid and the coefficients of thermal convection and implements them as boundary conditions. Validation of the aforementioned methods is done using the traditional thermal-network method that is based on analytical and empirical equations and this is the third method implemented in this paper. The comparison of the results between the different methods shows a very good agreement.

Keywords: High-speed permanent-magnet electrical machine; Thermal design; Computational fluid dynamics; Heat transfer

---

\* Corresponding author. Tel: +358 9 451 2382; fax: +358 9 451 2991. e-mail: zlatko.kolondzovski@tkk.fi

## 1. INTRODUCTION

The developed numerical techniques today give the opportunity for advanced thermal designs of high-speed permanent-magnet (PM) electrical machines. The temperature distribution at each point of the whole machine domain can be estimated and this gives an opportunity for finding the hot spots of the machine. Instead of using a rough empirical estimation of the mean convection, using the computational fluid dynamics (CFD), a more realistic modelling of the turbulent flow in the machine can be done, which leads to an advanced estimation of the heat transfer by convection from the machine parts to the cooling fluid. In fact, the complex machine geometry strongly influences the turbulence of the flow and more detailed turbulent analysis can be done in comparison with the empirical methods that are mostly referred to simple geometries.

There is a lack of references in which the numerical estimation of temperature distribution in an electrical machine is coupled with numerical estimation of the turbulent flow of the cooling fluid. In [1], a numerical thermal analysis of a conventional induction machine is done but the coefficients of thermal convection are calculated by empirical equations. In [2] and [3], an extensive numerical CFD approach for estimation of the turbulent fluid properties in the air gap in a high-speed induction machine is reported. The temperature rise of the fluid and the local coefficient of thermal convection in the air gap are determined and experimentally validated, but the temperatures of stator and rotor outer surfaces are accepted as constant values without estimation of the temperature distribution in the solid domain of the machine. If a complete numerical thermal analysis of the solid and fluid domains in a high-speed machine should be performed, the equations in the two domains must be solved simultaneously. One reason for this is that the temperature rise in the turbulent cooling

fluid and the temperatures in the solid machine parts are inherently dependent on each other. In fact, the temperature rise of the cooling fluid in a high-speed machine cannot be neglected since the coolant extracts a large amount of heat due to the very high loss density. That temperature rise in the cooling fluid contributes to an unequal temperature distribution in the machine, contributing the outlet side of the machine to be hotter than the inlet one. The temperature rise of the fluid also influences its turbulent properties and this is taken into account in the turbulent models.

In this paper, a multiphysics analysis of a high-speed PM machine is performed using the COMSOL Multiphysics<sup>®</sup> commercial software. The heat transfer and CFD modelling are performed simultaneously using a 2D axi-symmetric model of the machine. The final results for the temperature distribution in the solid domain of the machine are obtained using a 3D finite-element heat-transfer model. The results from the aforementioned numerical methods are validated using the traditional thermal-network method which is widely used and experimentally validated. For that purpose, a thermal network-model for the considered machine is created. The results for the temperature distribution from the numerical methods are very close when compared with the results obtained from the thermal-network method although the two methods are based on two completely different approaches.

The machine under consideration is a high-speed PM motor that is designed for speed  $n = 31.500$  rpm and power  $P = 130$  kW. The permanent magnets are mounted on an aluminium cage that shields the magnets from eddy-current heat generation. A carbon-fibre sleeve retains the magnets and the aluminium cage against the huge centrifugal forces that arise during the high-speed operation.

## 2. METHODS

### 2.1. 2D axi-symmetric numerical-multiphysics model

A multiphysics coupled CFD heat-transfer model is created for the simultaneous estimation of the temperature rise in the fluid and solid domains of the machine. The model is a 2D axi-symmetric one. The air flow in a high-speed PM machine is always turbulent. This is desired since in the case of turbulent flow the heat extraction due to convection is much more effective than in laminar flow. The turbulent model of the flow is performed using COMSOL Multiphysics<sup>®</sup> and the complete CFD analysis of this method is elaborated in [4]. The flow of an incompressible fluid is described by the Reynolds Averaged Navier-Stokes Equations (RANS)

$$\rho \frac{\partial \mathbf{U}}{\partial t} - \eta \nabla \cdot \nabla \mathbf{U} + \rho \mathbf{U} \cdot \nabla \mathbf{U} + \nabla P + \nabla (\overline{\rho \mathbf{u}' \otimes \mathbf{u}'}) = \mathbf{F} \quad (1)$$

$$\nabla \cdot \mathbf{U} = 0$$

where  $\eta$  denotes the dynamic viscosity,  $\mathbf{U}$  is the averaged velocity field,  $\mathbf{u}$  is the velocity vector,  $\rho$  is the density of the fluid,  $P$  is the pressure, and  $\mathbf{F}$  is the volumetric force vector. The last term on the left-hand side in the first equation represents fluctuations around a mean flow and it is called the Reynolds stress tensor. The  $\kappa$ - $\varepsilon$  turbulence model is used for the CFD analysis in this paper. This model gives a closure to the system and results in the following equations for the conservation of momentum and continuity

$$\rho \frac{\partial \mathbf{U}}{\partial t} - \nabla \cdot \left[ \left( \eta + \rho C_\mu \frac{\kappa^2}{\varepsilon} \right) \cdot (\nabla \mathbf{U} + (\nabla \mathbf{U})^T) \right] + \rho \mathbf{U} \cdot \nabla \mathbf{U} + \nabla P = \mathbf{F} \quad (2)$$

$$\nabla \cdot \mathbf{U} = 0$$

The two new variables in this equation are the turbulent kinetic energy  $\kappa$  and the dissipation rate of the turbulent energy  $\varepsilon$ . Two extra equations for  $\kappa$  and  $\varepsilon$  are solved for these two introduced variables

$$\begin{aligned} \rho \frac{\partial \kappa}{\partial t} - \nabla \cdot \left[ \left( \eta + \rho \frac{C_\mu \kappa^2}{\sigma_\kappa \varepsilon} \right) \nabla \kappa \right] + \rho \mathbf{U} \cdot \nabla \kappa &= \rho C_\mu \frac{\kappa^2}{2\varepsilon} \left( \nabla \mathbf{U} + (\nabla \mathbf{U})^T \right)^2 - \rho \varepsilon \\ \rho \frac{\partial \varepsilon}{\partial t} - \nabla \cdot \left[ \left( \eta + \rho \frac{C_\mu \kappa^2}{\sigma_\varepsilon \varepsilon} \right) \nabla \varepsilon \right] + \rho \mathbf{U} \cdot \nabla \varepsilon &= \rho C_{\varepsilon 1} \frac{\kappa}{2} \left( \nabla \mathbf{U} + (\nabla \mathbf{U})^T \right)^2 - \rho C_{\varepsilon 2} \frac{\varepsilon^2}{\kappa} \end{aligned} \quad (3)$$

The values of the model constants are:  $C_\mu = 0.09$ ,  $C_{\varepsilon 1} = 1.44$ ,  $C_{\varepsilon 2} = 1.92$ ,  $\sigma_\kappa = 0.9$  and  $\sigma_\varepsilon = 1.3$ . They are determined from experimental data.

The  $\kappa$ - $\varepsilon$  turbulence model gives an isotropic turbulence, which is a turbulence constant in all directions. However, close to solid walls the fluctuations in the turbulence vary greatly in magnitude and direction so in these places the turbulence cannot be considered as an isotropic one. The most convenient approach for modelling the properties of the thin boundary layer near the solid wall is by using an empirical relation between the values of velocity and wall friction. The complete set of boundary conditions for the solid wall is elaborated in [4]. The following boundary conditions for  $\kappa$  and  $\varepsilon$  are obtained

$$\kappa = \frac{u_\tau^2}{\sqrt{C_\mu}}; \quad \varepsilon = \frac{u_\tau^3}{k_a y} \quad (4)$$

where  $u_\tau$  is the friction velocity and  $k_a \approx 0.42$  is the Kármán's constant.

Besides the turbulent fluid flow, the application presented in this paper involves a thermal interaction of the flow and solid objects. In fact, when cooling the machine, heat is transferred from the hotter rotor and stator surfaces to the cooler air in the turbulent flow. In this case, a multiphysics coupling between the  $\kappa$ - $\varepsilon$  turbulence equations and heat-transfer equations is performed. The thermal conductivity of the fluid is automatically corrected to take into account the effect of mixing due to eddies.

The turbulence results in an effective thermal conductivity

$$k_{\text{eff}} = k_f + k_t; \quad k_t = C_p \eta_t \quad (5)$$

Here  $k_f$  is the physical thermal conductivity of the fluid,  $k_t$  is the turbulent conductivity,  $\eta_t$  is the turbulent cinematic viscosity and  $C_p$  is the heat capacity. According to [4], the laminar sub-layer is omitted in the analysis. The velocity, pressure and temperature fields are simultaneously solved in the presented multiphysics model.

The finite-element mesh of the 2D axi-symmetric geometry is presented in Figure 1. The mesh is refined on the boundaries between the solid and fluid domains and also close to the sharp corners. The idea of creating a 2D turbulent model was only to estimate the parameters of the air flow such as the temperatures of the flow and the coefficients of convection. These parameters valuable for the thermal behaviour of the machine can be used as input values in the 3D model. Building a 3D multiphysics model that couples CFD and heat-transfer analyses is not justified since the parameters of the flow like its temperature and coefficients of convection could be considered as constant ones in the third (tangential) direction. In addition, such a 3D model requires much higher computational resources, it is much more time consuming and could cause many problems in the solution procedure.

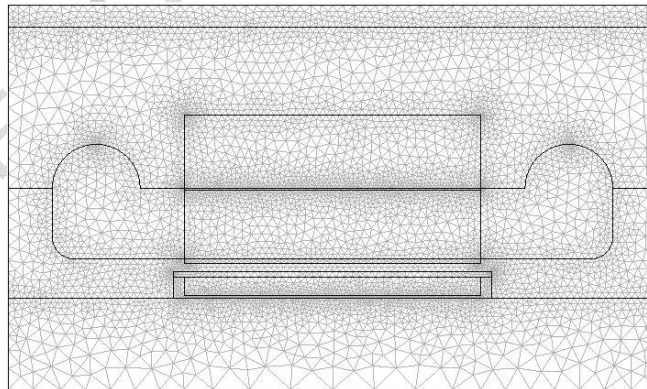


Figure 1: Finite-element mesh of the 2D axi-symmetric geometry of the high-speed PM machine

## 2.2. 3D numerical heat-transfer model

By introducing a 3-D thermal model of the machine, the temperatures in the whole solid domain of the machine can be estimated. The 3D numerical thermal analysis is performed using the COMSOL Multiphysics® software and is based on the FEM. The application of the FEM for solving heat-transfer problems is elaborated in [5]. The finite-element mesh of the 3D geometry of the machine is presented in Figure 2. The fluid domain is not modelled in the 3D heat-transfer model. The fluid parameters that influence the thermal behaviour of the machine like the fluid surface temperature and the heat transfer coefficients of convection are taken from the 2D multiphysics model and they represent input parameters for the boundary conditions of the 3D model. It means that the fluid effects in the 3D heat-transfer model are introduced as conditions on the boundaries on which the solid domain has an interaction with the fluid domain.

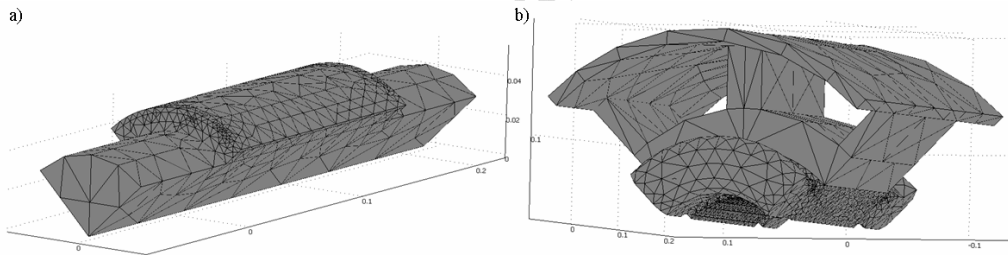


Figure 2: Finite-element mesh of the 3D geometry of the high-speed PM machine: a) rotor, b) stator

The outer boundary of the solid material in a contact with the cooling fluid is modelled using the boundary condition for the heat flux  $\mathbf{q}$

$$-\mathbf{n} \cdot \mathbf{q} = h(T_f - T) + q_0 \quad (6)$$

Here  $h$  is the heat-transfer coefficient of convection between the solid and fluid domain which is calculated using the 2D multiphysics model and  $T_f$  is the temperature of the fluid close to the solid wall. The term  $q_0$  is a general heat flux entering the domain. In our case, it models a general heat source on the solid surface such as the air friction

losses. The boundary condition which models an ideal thermal insulation or symmetry of the model is given by the equation

$$-\mathbf{n} \cdot \mathbf{q} = 0 \quad (7)$$

This condition is used for modelling the boundaries on which the solid domain is well insulated. This boundary condition is also used for reduction of the model size by taking advantage of the symmetry. The electrical machine that is under consideration is a 4-pole machine and only a quarter of the machine i.e. one pole pitch is modelled. Another boundary condition that is used is a prescribed constant temperature on a boundary

$$T = T_0 \quad (8)$$

This condition is used for modelling a boundary on which the temperature  $T_0$  is known in advance. The heat generation on a surface between two solid materials is modelled using the boundary condition

$$-\mathbf{n}_{\text{up}} \cdot (\mathbf{q}_{\text{up}} - \mathbf{q}_{\text{down}}) = q_0 \quad (9)$$

Here  $q_0$  is the generated heat flux on the surface. This equation states that the difference of the normal heat fluxes on the upper and lower side of the boundary are equal to the heat source. The eddy current losses on the surface of the magnets and the aluminium shield are modelled with the heat source  $q_0$ . If there is no heat generation on the boundary between two solid materials,  $q_0 = 0$ .

### 2.3. Thermal-network model

The thermal-network method uses traditional analytical and empirical approaches for determination of the temperature rises and here it serves just for comparison of its results with the results obtained by the numerical methods. The thermal network of the model is presented in Figure 3. It is based on the models given in [6], [7] and [8]. When solving the circuit model, the input parameters are: dimensions

and thermal properties of the machine parts, rotating speed, air-flow properties, ohmic losses in the windings and electromagnetic losses calculated previously by the FEM. The convection heat-transfer coefficients as well as the air-friction losses are calculated using analytical and empirical equations elaborated in [7] and [9]. Using the method reported in [10], the temperature rise in the fluid flow is also determined. In fact, in a high-speed machine, the temperature rise in the flow cannot be neglected as it is quite high because of the huge loss density in the machine. The circuit is solved for the temperatures at each node which in fact represent the average temperature rise in each part of the machine.

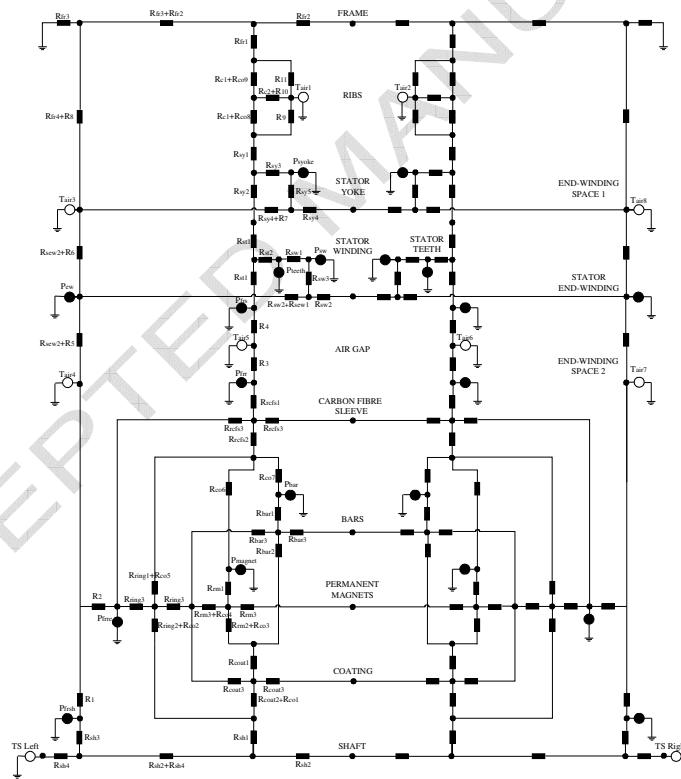


Figure 3: Thermal network of the high-speed PM machine

### 3. RESULTS AND DISCUSSION

#### 3.1. Results for the losses

The losses are the common input parameters for all the applied methods for determination of temperature distribution in the machine. The electromagnetic losses were calculated using FEM [11] and the mechanical losses were calculated with empirical equations [7]. One type of mechanical losses is due to the friction between the moving rotor surface and the air. Another type is due to the energy which is needed to blow the air through the machine because there is a friction between the air and the fluid passages. The results for all types of losses are presented in Table 1.

Table 1: Results for all types of losses in the machine

| Types of losses        |   | Power [W] |
|------------------------|---|-----------|
| Electromagnetic losses | Resistive losses in the permanent magnets | 123       |
|                        | Resistive losses in the aluminium cage    | 135       |
|                        | Resistive losses in the stator winding    | 936       |
|                        | Core losses in the stator yoke            | 223       |
|                        | Core losses in the stator teeth           | 355       |
| Mechanical losses      | Air-friction losses in the air gap        | 166       |
|                        | Air-friction losses on the rotor ends     | 72        |
|                        | Air-friction losses on the shaft ends     | 76        |
|                        | Air-friction losses in the fluid passages | 23        |

#### 3.2. Results for the temperature distribution in the machine

The 2D multiphysics method couples the equations from CFD and heat transfer so it gives a solution for the temperature distribution in the solid and fluid domains of the machine. A result of that temperature distribution is presented in Figure 4. The temperature distribution in the solid and fluid domains is not symmetrical. The temperature rise of the outlet side (the top of the figure) is higher than the temperature rise of the inlet side (the bottom of the figure).

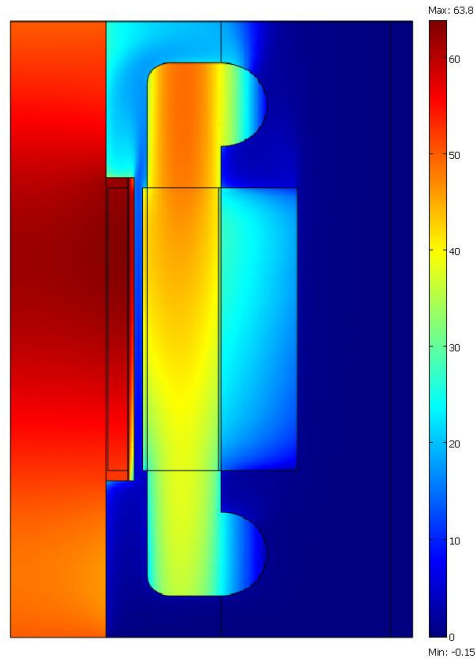


Figure 4: Distribution of the temperature rise  $\Delta T$  [K] in the solid and fluid domains of the electrical machine. The inlet side is on the bottom and the outlet side is on the top of the figure.

Since the 2D model gives quite rough results for the solid domain, the results of this method are primarily intended for estimating the properties of the fluid domain. Besides the temperature rise of the coolant, another important parameter that is obtained with this method is the coefficient of thermal convection on each surface between the solid and fluid domains. The local value of this coefficient is calculated in the postprocessor using the equation

$$h_{\text{local}} = \frac{q_{\text{local}}}{T_w - T_f} \quad (10)$$

Here  $q_{\text{local}}$  is the local heat flux,  $T_w$  is the local wall temperature of the solid domain and  $T_f$  is the local average temperature of the fluid next to the wall. In this way, all local heat-transfer coefficients of convection over all the outer surfaces of the solid domain in the machine are calculated.

The 3D heat transfer method serves for estimation of the temperature-rise distribution only in the solid domain of the machine. It gives a precise final 3D view of

the temperature rise distribution in all parts of the machine including those parts that cannot be successfully modelled with the 2D axi-symmetric model. Using boundary conditions for symmetry, only a quarter of the machine, i.e. one pole pitch, has been modelled. The temperature-rise distribution on the rotor boundaries is presented in Figure 5. Figure 6 presents the temperature-rise distribution of the inner rotor geometry. The temperature-rise distributions on the stator boundaries and the inner stator geometry are presented in Figures 7 and 8, respectively.

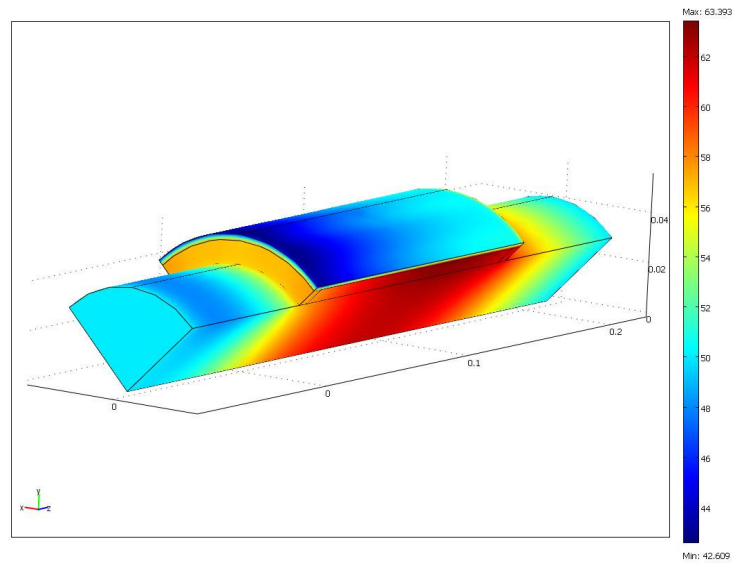


Figure 5: Distribution of the temperature rise  $\Delta T$  [K] on the rotor boundaries

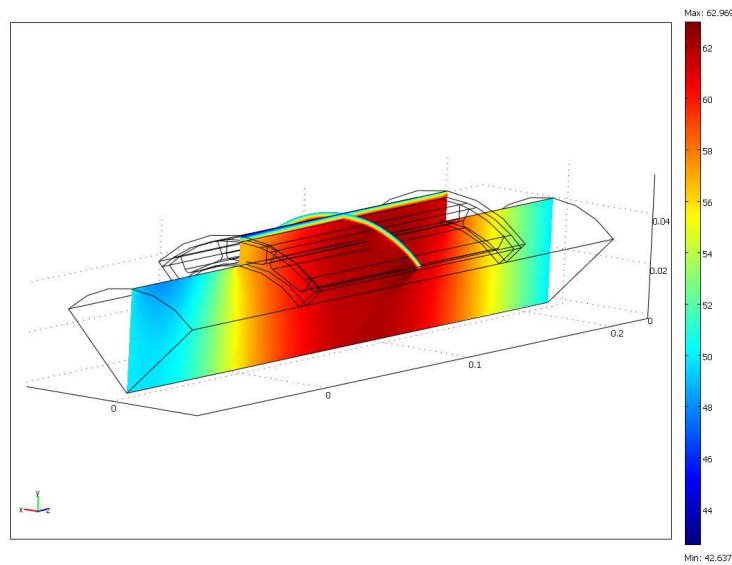


Figure 6: Distribution of the temperature rise  $\Delta T$  [K] of the inner rotor geometry

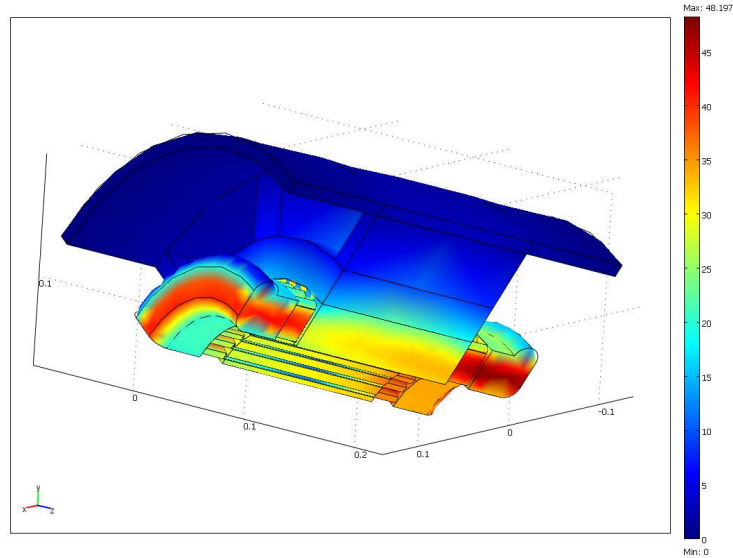


Figure 7: Distribution of the temperature rise  $\Delta T$  [K] on the stator boundaries

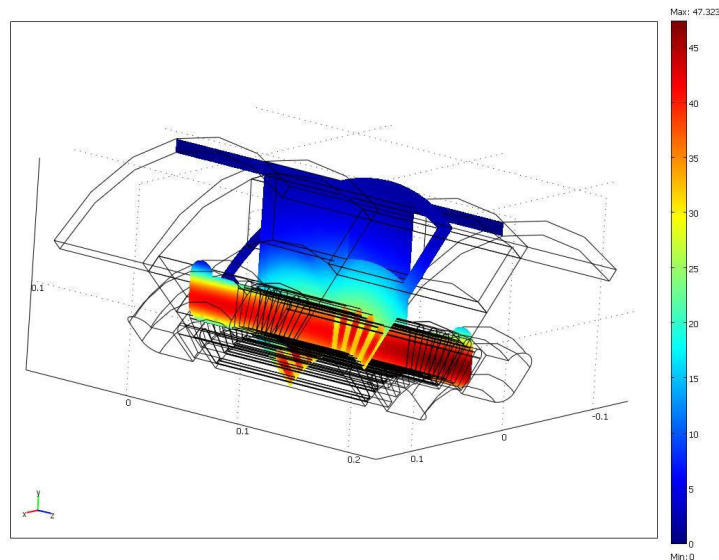


Figure 8: Distribution of the temperature rise  $\Delta T$  [K] of the inner stator geometry

### 3.3. Validation and discussion of the results

During the design process, the distribution of the temperature rise in the machine is estimated using 3 different methods: 2D multiphysics method, 3D heat-transfer method and a traditional thermal-network method. In the following, the results from the different methods will be compared. The thermal-network method will be considered as a reference one since it is a traditional method that is proved and validated with test

measurements in many references. Since the 3D heat-transfer method for estimation of the temperature rise in the solid-part of the machine is dependent on the 2D multiphysics method, these two methods can be considered as a one numerical-multiphysics method. The final results for temperature rises in all solid parts of the electrical machine are obtained from the 3D heat-transfer method and these results are compared with the results obtained from the thermal-network method. The comparison of the results for the temperature rises in all parts of the electrical machine is presented in Figure 9. The comparison shows a very good agreement between the results. The best agreement between the results is achieved when the estimated temperature rises in the aluminium cage, permanent magnets and carbon-fibre sleeve are compared. In all other machine parts, the differences between the estimated values for temperature rises do not exceed 5K. The small deviations among the results are due to the different nature of the implemented methods and the vagueness in the determination of the coefficients of thermal convection. The implemented methods predict that the temperatures in the most sensitive thermal parts of the machine are lower than their critical values. This means that the machine under design fulfils all the thermal constraints.

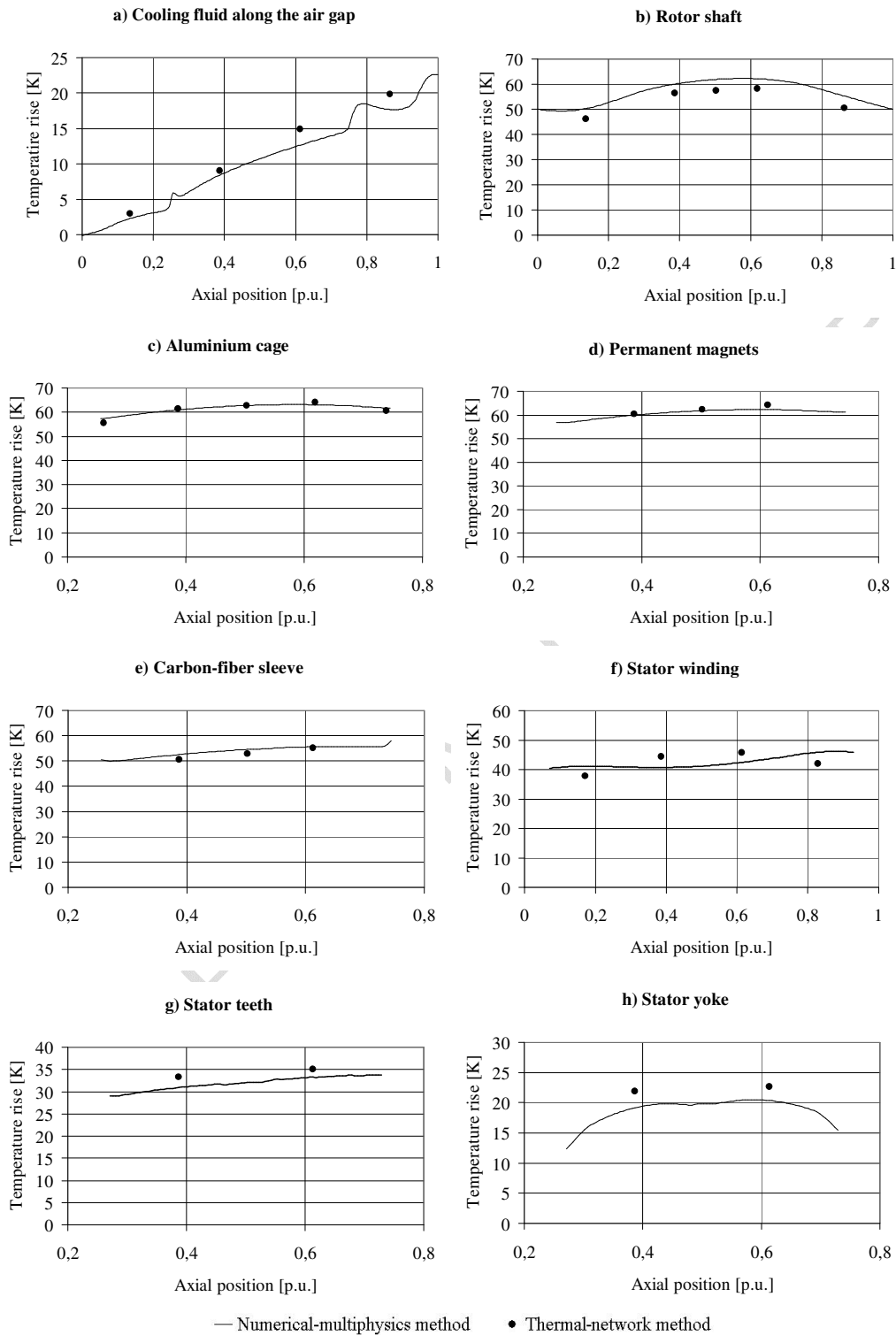


Figure 9: Comparison of the results for the temperature rise in different parts in the machine predicted by the numerical-multiphysics method and the thermal-network method

#### 4. CONCLUSION

An accurate measurement of the temperatures in a high-speed PM machine is very difficult since the rotor is rotating in operation (would require a telemetry unit). That is why reliable theoretical methods for accurate prediction of the temperature distribution in the whole machine domain should be developed. In this paper, a combined 2D-3D finite-element thermal analysis of the electrical machine is presented. First, using a 2D multiphysics method, the thermal properties of the flow such as the coefficient of thermal convection and temperature rise of the flow were estimated. The distribution of the temperature rise in the whole solid domain of the machine was determined by the 3D numerical heat-transfer method. The results for the temperature rises in the machine from the aforementioned methods are compared with the results obtained by the thermal-network method that uses a totally different approach in the heat-transfer analysis. The presented numerical method is a novel compromise between the 2D axy-symmetric multiphysics rough modelling and the 3D thermal fine modelling, a compromise that allows an accurate estimation of the local temperature rises with a minimum amount of computational resources.

## References:

- [1] Y. Huai, R.V.N. Melnik, P.B. Thogersen, Computational analysis of temperature rise phenomena in electric induction motors, *Applied Thermal Engineering* 23 (7) (2003) 779-795.
- [2] M. Kuosa, P.Salinen, J. Larjola, Numerical and experimental modeling of gas flow and heat transfer in the air gap of an electric machine, *Journal of Thermal Science* 13 (3) (2004) 264-278.
- [3] M. Kuosa, P.Salinen, A. Reunanen, J. Backman, J. Larjola, L. Koskelainen, Numerical and experimental modelling of gas flow and heat transfer in the air gap of an electric machine. PartII: Grooved surfaces, *Journal of Thermal Science* 14 (1) (2005) 48-55.
- [4] Comsol Multiphysics, Heat Transfer Module, User's Guide, Version 3.3, 2006.
- [5] W.J. Minkowycz, E. M. Sparrow, J. Y. Murthy, *Hanbook of Numerical Heat Transfer*, 2<sup>nd</sup> Edition, Wiley, USA, 2006.
- [6] P.H. Melor, D. Roberts, D.R. Turner, Lumped parameter thermal model for electrical machines of TEFC design, *IEE Proceedings-B* 138 (5) (1991) 205-218.
- [7] J. Saari, *Thermal Modelling of High-Speed Induction Machines*, Acta Polytechnica Scandinavica, Helsinki, 1995.
- [8] J. Saari, *Thermal Analysis of High-Speed Induction Machines*, Acta Polytechnica Scandinavica, Espoo, 1998.
- [9] F.P. Incropera, D.P. DeWitt, *Fundamentals of Heat and Mass Transfer*, Third edition, John Wiley and sons, USA, 1990.
- [10] T. Jokinen, J. Saari, Modelling of the coolant flow with heat flow controlled temperature sources in the thermal networks, *IEE Proceedings* 144 (5) (1997) 338-342.
- [11] A. Arkkio, *Analysis of Induction Motors Based on the Numerical Solution of the Magnetic Field and Circuit Equations*, Acta Polytechnica Scandinavica, Helsinki, 1987.

Figure captions and legends:

Figure 1: Finite element mesh of the 2D geometry of the high-speed PM machine

Figure 2: Finite element mesh of the 3D geometry of the high-speed PM machine: a) rotor, b) stator

Figure 3: Thermal network of the high-speed PM machine

Figure 4: Distribution of the temperature rise  $\Delta T$  [K] in the solid and fluid domains of the electrical machine. The inlet side is on the bottom and the outlet side is on the top of the figure.

Figure 5: Distribution of the temperature rise  $\Delta T$  [K] on the rotor boundaries

Figure 6: Distribution of the temperature rise  $\Delta T$  [K] of the inner rotor geometry

Figure 7: Distribution of the temperature rise  $\Delta T$  [K] on the stator boundaries

Figure 8: Distribution of the temperature rise  $\Delta T$  [K] of the inner stator geometry

The legend for Figure 9: — Numerical-multiphysics method    • Thermal-network method

Figure 9: Comparison of the results for the temperature rise in different parts in the machine predicted by the numerical-multiphysics method and the thermal-network method

#### Tables:

Table 1: Results for all types of losses in the machine

| Types of losses        |   | Power [W] |
|------------------------|---|-----------|
| Electromagnetic losses | Resistive losses in the permanent magnets | 123       |
|                        | Resistive losses in the aluminium cage    | 135       |
|                        | Resistive losses in the stator winding    | 936       |
|                        | Core losses in the stator yoke            | 223       |
|                        | Core losses in the stator teeth           | 355       |
| Mechanical losses      | Air-friction losses in the air gap        | 166       |
|                        | Air-friction losses on the rotor ends     | 72        |
|                        | Air-friction losses on the shaft ends     | 76        |
|                        | Air-friction losses in the fluid passages | 23        |

**Nomenclature**

|                     |   |
|---------------------|---|
| $C_p$               | heat capacity, J/(kg·K)                                 |
| $C_\mu$             | model constant  |
| $C_{\varepsilon 1}$ | model constant  |
| $C_{\varepsilon 2}$ | model constant  |
| $F$                 | volumetric force vector, N                              |
| $h$                 | heat-transfer coefficient, W/(m <sup>2</sup> ·K)        |
| $h_{\text{local}}$  | local heat-transfer coefficient, W/(m <sup>2</sup> ·K)  |
| $k_{\text{eff}}$    | effective thermal conductivity, W/(m·K)                 |
| $k_a$               | Kármán's constant                                       |
| $k_c$               | physical thermal conductivity of the fluid, W/(m·K)     |
| $k_t$               | turbulent conductivity W/(m·K)                          |
| $n$                 | rectangular unit vector                                 |
| $P$                 | pressure, Pa  |
| $q$                 | heat flux, W/m <sup>2</sup>                             |
| $q_0$               | general heat flux entering the domain, W/m <sup>2</sup> |
| $q_{\text{local}}$  | local heat flux, W/m <sup>2</sup>                       |
| $T$                 | temperature, K  |
| $T_0$               | prescribed temperature on a boundary, K                 |
| $T_f$               | temperature of the fluid, K                             |
| $T_w$               | temperature of the wall, K                              |
| $t$                 | time, s   |
| $U$                 | averaged velocity field, m/s                            |
| $u$                 | velocity vector, m/s                                    |
| $u_\tau$            | friction velocity, m/s                                  |
| $y$                 | normal distance from the wall, m                        |

*Greek symbols*

|                      |   |
|----------------------|---|
| $\varepsilon$        | dissipation rate of $\kappa$ , m <sup>2</sup> /s <sup>3</sup> |
| $\eta$               | dynamic viscosity, Pa·s                                       |
| $\eta_t$             | turbulent cinematic viscosity, m <sup>2</sup> /s              |
| $\kappa$             | turbulent kinetic energy, m <sup>2</sup> /s <sup>2</sup>      |
| $\rho$               | density of the fluid, kg/m <sup>3</sup>                       |
| $\sigma_\kappa$      | model constant  |
| $\sigma_\varepsilon$ | model constant  |

*Subscripts and abbreviations*

|      |                  |
|------|------------------|
| down | down side        |
| eff  | effective        |
| f    | fluid            |
| PM   | permanent magnet |
| t    | turbulent        |
| up   | upper side       |
| w    | wall             |